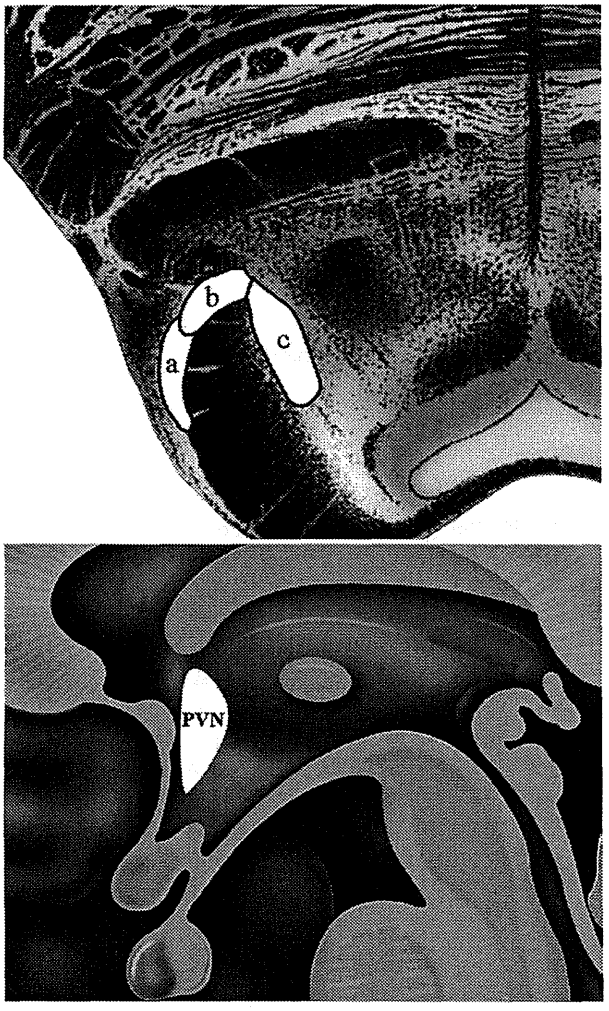

FIG. 3. **Upper:** The parabrachial area is composed of the lateral PBN (a), the Kölliker-Fuse nucleus (b), and the medial PBN (c). **Lower:** The PVN is localized in the medial hypothalamus.

per pons, and this condition was resolved after surgery. These findings suggested that the intractable yawning might have resulted from the tumor compressing the PBN located on the dorsal side of the junction of the midbrain and pons.

Disclosure

The authors report no conflict of interest concerning the materials or methods used in this study or the findings specified in this paper.

Author contributions to the study and manuscript preparation include the following. Conception and design: Saura, Beppu. Analysis and interpretation of data: Uesugi, Sasaki. Critically revising the article: all authors. Reviewed submitted version of manuscript: all authors. Approved the final version of the manuscript on behalf of all authors: Saura. Administrative/technical/material support: Matsuura, Asahi.

References

1. Arai K, Kita K, Komiyama A, Hirayama K, Saeki N, Nagao K: [Progressive dysautonomia in hemangioblastoma in the region of the fourth ventricle.] **No To Shinkei 38:**195–200, 1986 (Jpn)
2. Blair ML, Piekut D, Want A, Olschowka JA: Role of the hypothalamic paraventricular nucleus in cardiovascular regulation. **Clin Exp Pharmacol Physiol 23:**161–165, 1996
3. Cronin TG Jr: Yawning: an early manifestation of vasovagal reflex. **AJR Am J Roentgenol 150:**209, 1988 (Letter)
4. Honda K, Higuchi T: Role of midbrain parabrachial nucleus in controlling electrical activity of oxytocin and vasopressin secreting neurones in the hypothalamic supraoptic nucleus. **J Reprod Dev 47:**259–265, 2001
5. Kiernan JA: **Barr's The Human Nervous System: An Anatomical Viewpoint, ed 9.** Baltimore: Lippincott Williams & Wilkins, 2009, pp 147–148
6. Kita I, Sato-Suzuki I, Oguri M, Arita H: Yawning responses induced by local hypoxia in the paraventricular nucleus of the rat. **Behav Brain Res 117:**119–126, 2000
7. Naidich TP, Duvernoy HM, Delman BN, Sorensen AG, Kollias SS, Haacke EM: **Duvernoy's Atlas of the Human Brain Stem and Cerebellum: High-Field MRI: Surface Anatomy, Internal Structure, Vascularization and 3D Sectional Anatomy.** New York: Springer, 2009, p 324
8. Sato-Suzuki I, Kita I, Oguri M, Arita H: Stereotyped yawning responses induced by electrical and chemical stimulation of paraventricular nucleus of the rat. **J Neurophysiol 80:**2765–2775, 1998
9. Ueyama T, Senba E: [Limbic system and autonomic nervous system.] **Rinsho Shinkeigaku 50:**1003–1006, 2010 (Jpn)

Manuscript submitted October 11, 2013.
Accepted April 30, 2014.
Please include this information when citing this paper: published online May 30, 2014; DOI: 10.3171/2014.4.JNS132243.
Address correspondence to: Hiroaki Saura, M.D., Department of Neurosurgery, Iwate Medical University, 19-1 Uchimaru, Morioka 020-8505, Japan. email: hirosau@gmail.com.

Kanemoto et al. BMC Cancer 2014, 14:641
http://www.biomedcentral.com/1471-2407/14/641

BMC Cancer

RESEARCH ARTICLE Open Access

Prognostic prediction of glioblastoma by quantitative assessment of the methylation status of the entire *MGMT* promoter region

Manabu Kanemoto[1,2], Mitsuaki Shirahata[3], Akiyo Nakauma[1], Katsumi Nakanishi[1], Kazuya Taniguchi[1], Yoji Kukita[1], Yoshiki Arakawa[2], Susumu Miyamoto[2] and Kikuya Kato[1*]

Abstract

Background: O6-methylguanine-DNA methyltransferase (*MGMT*) promoter methylation is reported to be a prognostic and predictive factor of alkylating chemotherapy for glioblastoma patients. Methylation specific PCR (MSP) has been most commonly used when the methylation status of *MGMT* is assessed. However, technical obstacles have hampered the implementation of MSP-based diagnostic tests. We quantitatively analyzed the methylation status of the entire *MGMT* promoter region and applied this information for prognostic prediction using sequencing technology.

Methods: Between 1998 and 2012, the genomic DNA of 85 tumor samples from newly diagnosed glioblastoma patients was subjected to bisulfite treatment and subdivided into a training set, consisting of fifty-three samples, and a test set, consisting of thirty-two samples. The training set was analyzed by deep Sanger sequencing with a sequencing coverage of up to 96 clones per sample. This analysis quantitatively revealed the degree of methylation of each cytidine phosphate guanosine (CpG) site. Based on these data, we constructed a prognostic prediction system for glioblastoma patients using a supervised learning method. We then validated this prediction system by deep sequencing with a next-generation sequencer using a test set of 32 samples.

Results: The methylation status of the *MGMT* promoter was correlated with progression-free survival (PFS) in our patient population in the training set. The degree of correlation differed among the CpG sites. Using the data from the top twenty CpG sites, we constructed a prediction system for overall survival (OS) and PFS. The system successfully classified patients into good and poor prognosis groups in both the training set (OS, $p = 0.0381$; PFS, $p = 0.00122$) and the test set (OS, $p = 0.0476$; PFS, $p = 0.0376$). Conventional MSP could not predict the prognosis in either of our sets. (training set: OS; $p = 0.993$ PFS; $p = 0.113$, test set: OS; $p = 0.326$ PFS; $p = 0.342$).

Conclusions: The prognostic ability of our prediction system using sequencing data was better than that of methylation-specific PCR (MSP). Advances in sequencing technologies will make this approach a plausible option for diagnoses based on *MGMT* promotor methylation.

Keywords: Glioma, O6-methylguanine-DNA methyltransferase, Methylation, Bisulfite genome sequencing, Next-generation sequencing

* Correspondence: katou-ki@mc.pref.osaka.jp
[1]Research Institute, Osaka Medical Center for Cancer and Cardiovascular Diseases, 1-3-3 Nakamichi, Higashinari-ku, Osaka, Japan
Full list of author information is available at the end of the article

Background

A glioblastoma (GB) is a malignant brain tumor with a poor prognosis; the median survival time of GB patients is less than 2 years [1]. The current standard of care for GB patients is maximum surgical resection combined with radiation and concomitant adjuvant temozolomide (TMZ) therapy [2]. The long-term results of the EORTC-NCIC CE.3 trial revealed that the 5-year survival of GB patients approaches 10%, despite the largely poor prognosis [3]. Although novel drugs, such as molecular-targeted drugs, have been developed, their survival benefit has not been confirmed, and these molecular targeted drugs are known to carry risks of specific adverse events [4-6]. Accordingly, it is important to identify patients who may respond to conventional chemo-radiation therapy as part of future personalized care. Although nitrosoureas were commonly used for chemotherapy, TMZ is now used for first-line therapy. These drugs are alkylating agents that add an alkyl group to the O6 position of guanine, damaging the genomic DNA of cancer cells. O6-methylguanine-DNA methyltransferase (MGMT) removes alkyl groups from the O6 position of guanine and plays an important role in DNA repair [7-10]. Therefore, *MGMT* expression is associated with resistance to chemotherapeutic alkylating agents. The expression of *MGMT* is controlled by epigenetic gene silencing [11-13]. The methylation of the *MGMT* promoter is associated with sensitivity to alkylating chemotherapy drugs and is recognized as a prognostic factor for GB patients [14-18].

In recent years, TMZ monotherapy has been attempted for elderly GB or low-grade glioma patients, and an association between the treatment response and the *MGMT* methylation status has been examined [19,20]. These studies demonstrated that the methylation status of *MGMT* is a strong predictive factor of TMZ monotherapy outcomes in elderly GB patients, and the clinical utility of the *MGMT* methylation status is increasing [21,22].

Even with this accumulating clinical evidence, the implementation of diagnostic tests examining the methylation status of the *MGMT* promoter has been difficult. PCR-based techniques, such as methylation-specific PCR (MSP) and quantitative MSP, are the most popular methods of assessment [23,24]. These techniques detect methylation sequences by sequence-specific binding of primers, which is an indirect method and only detects a limited number of methylation sites. DNA sequencing (i.e., bisulfite genomic sequencing) provides more direct information on methylation status. In this context, pyrosequencing is considered a good alternative. However, the target methylation sites of pyrosequencing are also limited [25,26]. The *MGMT* promoter region spans more than one thousand base pairs and contains approximately one hundred potential methylation sites. To assess the methylation status of the *MGMT* promoter, it would be preferable to assess information from all methylation sites and select important CpG sites with survival analysis.

In this report, we performed deep sequencing of the *MGMT* promoter region after bisulfite treatment to clarify the global methylation status of the region. Because the methylation status is not uniform in glioma tissue, it is important to characterize the intratumor heterogeneity of *MGMT* promoter methylation. An analysis of survival data assessed the correlation between each CpG site and the malignancy of the glioblastoma. Based on this correlation, we built a classifier to predict the malignancy of GB using deep sequencing with a next-generation sequencer.

Methods

Patient characteristics

We obtained 85 GB specimens from patients who underwent surgical resection at Kyoto University Hospital and related regional hospitals between 1998 and 2012. The majority of the patients were recruited for a phase II clinical trial [27], and their tissues were used for studies on gene expression profiling [28,29]. Histological diagnoses were established by the Kyoto University Pathology Unit according to the criteria established by the World Health Organization. The protocol was approved by the institutional review board of Kyoto University, and written informed consent was obtained from each of the patients. All tumor specimens were immediately snap frozen upon surgical resection and stored at −80°C until use. Tumor specimens containing 20% or more non-tumor tissue or necrotic areas were excluded from further analysis. The preoperative Karnofsky performance status score of each patient was at least 50 for each case. All patients received radiation therapy with and without alkylating chemotherapy postoperatively. The patient characteristics are shown in Table 1. We divided the data matrix into two data sets: one set consisted of 53 patients and was designated as the training set, and the other set contained 32 patients and was designated as the test set.

DNA extraction and bisulfite treatment

Genomic DNA was extracted with the QIAamp DNA Mini Kit (Qiagen) according to the manufacturer's instructions. One nanogram of genomic DNA was subjected to bisulfite treatment using the MethylEasy DNA Bisulfite Modification Kit (Takara) in accordance with the manufacturer's instructions. We determined the quality of bisulfite-treated genomic DNA by real-time PCR of the actin gene as previously described [30]. The outline of the procedure is schematically shown in Additional file 1: Figure S1.

Table 1 Patients' clinical characteristics

Sample		85	
Age		6-88	Median: 60
Gender	Female	36	
	Male	49	
Removal	Biopsy	1	
	Partial	29	
	Subtotal	28	
	Total	20	
	Unknown	8	
Post operative therapy	VAC-feron	57	
	Temozolomide	14	
	Other ACNU regimen	4	
	Radiation alone	7	
	Other	3	
Overall survival (months)		3-96	Median: 12
Progression free survival (months)		1-96	Median: 6

Methylation-specific PCR (MSP)

Conventional MSP was performed as previously described [31]. PCR was performed using AmpliTaq Gold polymerase and the GeneAmp PCR system 9700 (Applied Biosystems). The sequences of the primer pairs were 5′-TTTGTGTTTTGATGTTTGTAGGTTTTTGT-3′ and 5′-AACTCCACACTCTTCCAAAAACAAAACA-3′ for unmethylated *MGMT* (fragment size: 93 bp) and 5′- TTTCGACGTTCGTAGGTTTTCGC -3′ and 5′-GCA CTCTTCCGAAAACGAAACG-3′ for methylated *MGMT* (fragment size: 81 bp). These sequences and the PCR primer sequences used in the further analysis were constructed according to the *MGMT* promoter sequence (http://www.ncbi.nlm.nih.gov/nuccore/X61657.1). After an initial incubation at 95°C for 12 min, PCR amplification was performed with 40 cycles of 95°C for 15 sec, 59°C for 30 sec, and 72°C for 30 sec, followed by a 4-min final extension. The PCR products were electrophoresed on 2% agarose gels and were classified as methylated if a band with the PCR product was visualized using the methylated primer. The experiments were performed twice to confirm the reproducibility of the results. There were no discrepancies between duplicate reactions.

Quantitative bisulfite genome sequencing (qBGS) of the training set

For qBGS, the *MGMT* promoter region was amplified by nested PCR. The sequences of the first-round PCR primers were 5′-TGGTAAATTAAGGTATAGAGTTTT AGG-3′ and 5′-GGTTAGGTGTTAGTGATGTT-3′. The PCR protocol was optimized for bisulfite-treated genomic DNA; each 10-μl reaction mixture of the modified protocol contained 2.5 mM $MgCl_2$, 3% DMSO, 20 ng bisulfite-treated genomic DNA, and 1 μl of AmpliTaq Gold. After an initial incubation at 95°C for 12 min, PCR amplification was performed using 30 cycles of 95°C for 15 sec, 54°C for 30 sec and 72°C for 1 min, followed by a 4-min final extension. A 1-μl aliquot of the first-round PCR product was used as the template of the second-round PCR reaction. The sequences of the second-round PCR primers were 5′-TGGTAAATTAAGGTATAGAGTTTTAGG-3′ and 5′-TT GGATTAGGTTTTTGGGGTT-3′ (fragment size: 662 bp). The genomic position is chr 10: 131,155,100-131,155,761. The second-round PCR was performed using KOD-plus DNA polymerase (TOYOBO) according to the manufacturer's instructions with 1.5 mM $MgSO_4$ and 3% DMSO. After an initial incubation at 95°C for 2 min, PCR amplification was performed with 30 cycles of 94°C for 15 sec, 58°C for 30 sec, and 68°C for 1 min. The PCR products were purified using the MinElute PCR Purification Kit (QIAGEN) and ligated into the pCR-Blunt plasmid using the Zero Blunt PCR Cloning Kit (Invitrogen) and a DNA ligation kit (Takara). MAX Efficiency DH5 Competent Cells (Invitrogen) were used for transformations. A total of 96 colonies of each sample were subjected to bisulfite sequencing using a 3730xl DNA Analyzer (Applied Biosystems). The methylation status was analyzed with QUMA web tools (http://quma.cdb.riken.jp/).

qBGS for the test set

For the test set, we used next-generation sequencing (MiSeq, Illumina) instead of Sanger sequencing. The target sequence was amplified by nested PCR. PCR amplification was performed using 40 cycles of 94°C for 30 sec, 54°C for 30 sec, and 72°C for 45 min, followed by a 4-min final extension. The sequences of the first-round PCR primers were 5′-GGATATGTTGGGATAGTT-3′ and 5′-CCAAAAACCCCAAACCC-3′ [26]. The sequences of the second-round PCR primers were 5′-GGATATGTTGGGATAGTT-3′ and 5′- AAATAAATAA AAATCAAAAC-3′ (fragment size: 216 bp). The annealing temperature was 48°C in the second-round PCR. The PCR product was attached with an adapter for MiSeq plus, consisting of an eight- or six-base index. The pooled PCR library of the test set samples was sequenced by paired-end sequencing with a MiSeq sequencer. Paired-end reads were aligned to a C-to-T converted reference sequence of the *MGMT* promoter region using BWA [32]. We used SAMtools to obtain the per-base coverage (pileup files) and counted non-bisulfite converted sites [33].

Statistical analysis

Statistical analyses were performed using the free statistics software R (http://www.r-project.org/). Overall survival (OS) and progression-free survival (PFS) were defined as the period from surgery to death and from surgery to radiological detection of tumor progression,

respectively. Tumor progression was diagnosed based on the criteria of the Brain Tumor Registry committee (Japan), which includes: a 25% increase in tumor size, the appearance of new lesions, or the obvious deterioration of the patient due to a mass effect or perifocal edema (in Table 1).

Results

Quantitative bisulfite genome sequencing of the training set

Bisulfite sequencing was performed to fully analyze the methylation status of the *MGMT* promoter region. Due to intratumor heterogeneity, the methylation status of individual cells is not identical, even within a single glioma tissue. To clarify this heterogeneity, we performed quantitative bisulfite sequencing and obtained data from 25 to 81 molecules (median, 51) from each sample. This approach is referred to as quantitative bisulfite genome sequencing (qBGS). The 662-bp fragment subjected to qBGS contained 78 CpG sites. One CpG site that is not located within the CpG island of the *MGMT* promoter region was excluded from further analysis. The methylation proportion at each CpG site was calculated as the fraction of clones with a methylated C at that site in all sequenced clones. The methylation status of the *MGMT* promoter region was then described as a data point in a 77-dimensional space constructed from the methylation proportions of the 77 CpG sites. We performed a hierarchical cluster analysis with the Ward method using the raw methylation proportion without any standardization to obtain a general view of the global methylation features of the *MGMT* promoter region. The cases were grouped into four clusters (Figure 1A). These clusters were correlated with the degree of methylation. The column bars below the clustering indicate the MSP results for 53 samples. Typical examples of qBGS results are shown in Figure 2. The samples in cluster 1 were strongly methylated, the samples in cluster 2 were moderately methylated, the samples in cluster 3 were slightly methylated, and the samples in cluster 4 were almost

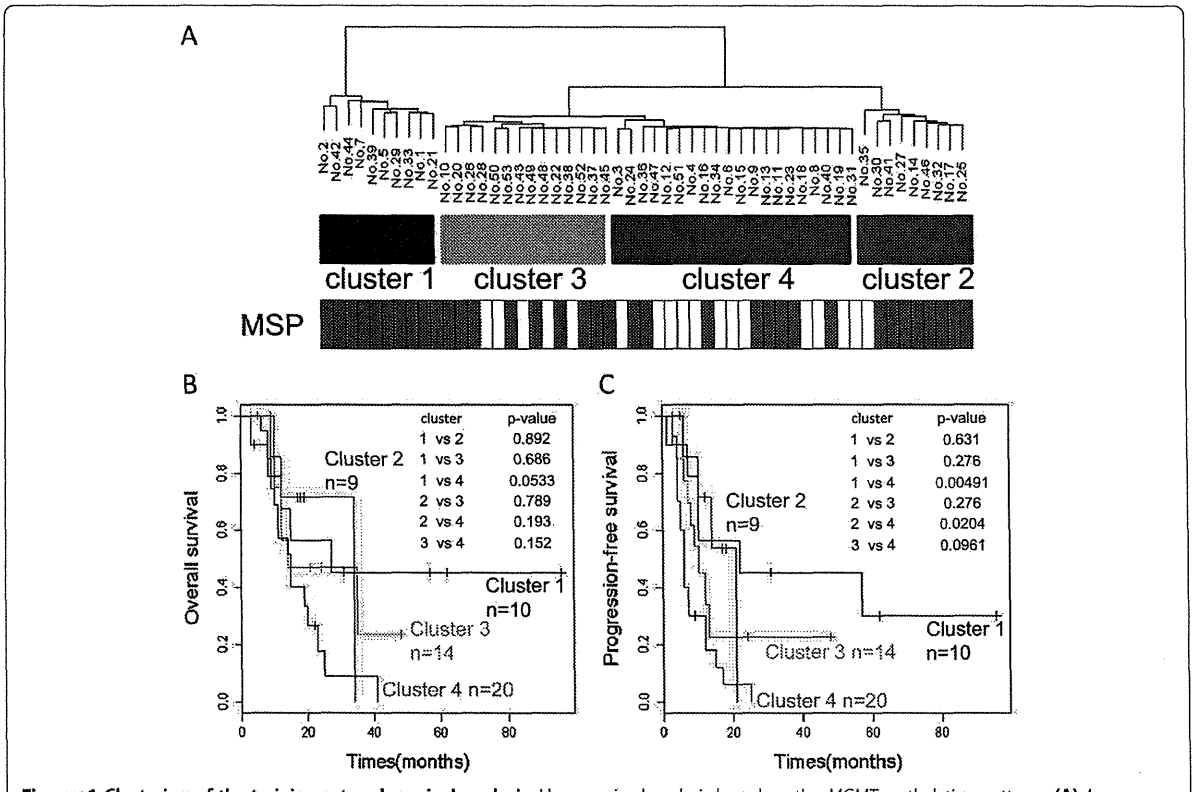

Figure 1 Clustering of the training set and survival analysis. Unsupervised analysis based on the *MGMT* methylation patterns. **(A)** A hierarchical cluster analysis of the methylation of the MGMT promoter in 53 samples. Cluster 1 (Black), strongly methylated samples; cluster 2 (red), moderately methylated; cluster 3 (green), slightly methylated; cluster 4 (blue), mostly unmethylated. The columns below the clustering show the results obtained using MSP. The gray column indicates methylated, and the white column is unmethylated samples. **(B, C)** Survival analysis was performed between all combinations of the four cluster subgroups. For PFS, the analysis showed statistically significant differences between cluster 1 and cluster 4 ($p = 0.00491$) and between cluster 2 and cluster 4 ($p = 0.0204$). For OS, there was no statistically significant difference between any combination of the four clusters, but there was a trend toward a difference between cluster 1 and cluster 4 ($p = 0.0533$).

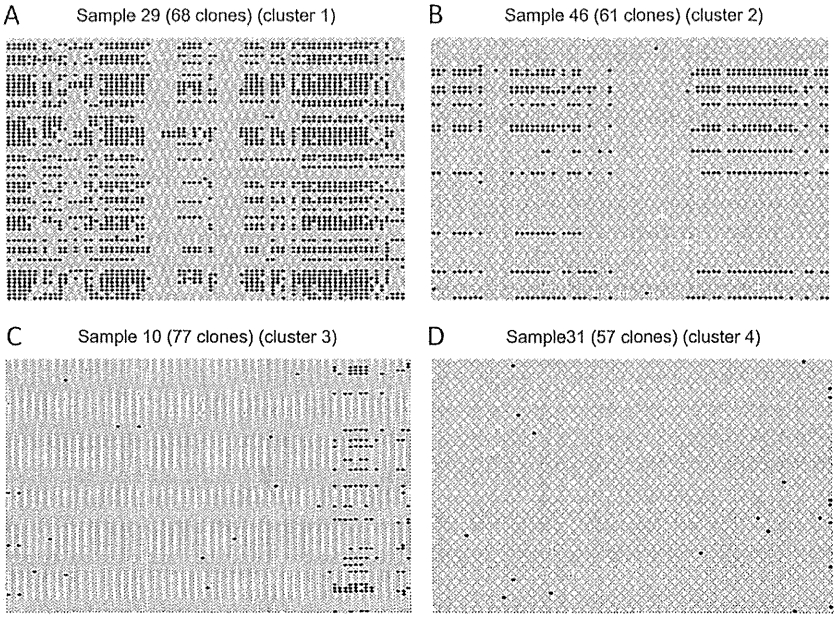

Figure 2 Methylation pattern obtained by qBGS. Methylation pattern observed using qBGS. The black and white circles indicate methylated and unmethylated CpG sites, respectively. Horizontally, 77 CpG sites are aligned. Vertically, the sequencing results of individual clones are aligned. **(A)** Sample 29 from cluster 1 of Figure 1; **(B)** sample 46 from cluster 2; **(C)** sample 10 from cluster 3; and **(D)** sample 31 from cluster 4.

unmethylated. There was a trend toward a prognostic difference for OS between cluster 1 and cluster 4 ($p = 0.0533$) (Figure 1B). Statistically significant associations with PFS were observed between clusters 1 and 4 ($p = 0.00491$) and between clusters 2 and 4 ($p = 0.0204$) (Figure 1C). Several cases that were judged to be methylated (i.e., to have a good prognosis) by MSP belonged to clusters 3 and 4 (Figure 1A). For example, samples 13 and 16 belonged to cluster 4; both showed four months of PFS and were described as poor prognosis [2], but were judged to be methylated and to have a good prognosis by MSP.

To demonstrate an overview of the methylation status of the *MGMT* promoter region, the averages of the methylation proportions of the CpG sites are shown in Figure 3. The promoter sequence may be divided into three segments according to the methylation proportions. The methylation level of the CpG sites in the middle segment, from CpG28 to CpG50, was lower than that of the other segments (Figure 3). This area is located just upstream of the transcription start site. We performed univariate Cox proportional hazard analysis of PFS to identify prognostically important CpG sites using the methylation proportion as a continuous variable. Based on an analysis using the 53 training samples, the log-rank p values of 20 CpG sites were less than 0.05. These 20 selected CpG sites were CpG63 ($p = 0.0056$), CpG64 ($p = 0.0088$), CpG77 ($p = 0.010$), CpG62 ($p = 0.012$), CpG56 ($p = 0.012$), CpG68 ($p = 0.014$), CpG11 ($p = 0.023$), CpG65 ($p = 0.025$), CpG66 ($p = 0.025$), CpG59 ($p = 0.027$), CpG8 ($p = 0.028$), CpG60 ($p = 0.028$), CpG10 ($p = 0.030$), CpG7 ($p = 0.034$),CpG5 ($p = 0.034$), CpG61 ($p = 0.035$), CpG54 ($p = 0.038$), CpG9 ($p = 0.038$), CpG47 ($p = 0.047$), and CpG67 ($p = 0.048$). Almost all of the selected sites were located at positions from CpG5 to CpG11 or from CpG54 to CpG68 (black columns in Figure 3). However, only five CpG sites were selected for OS under the same condition: CpG8 ($p = 0.039$), CpG28 ($p = 0.041$), CpG56 ($p = 0.041$), CpG5 ($p = 0.044$), and CpG45 ($p = 0.049$) (gray columns in Figure 3). Three CpG sites, CpG5, CpG8, and CpG56, showed a correlation with OS and PFS. All of the results of univariate Cox analysis are supplied in Additional file 2 (PFS) and Additional file 3 (OS). Shah et al. reported a similar comprehensive methylation analysis [34]. Their numbering scheme of CpG sites corresponds to the addition of twenty to our numbering scheme of sites.

Diagnostic system for prognosis prediction using quantitative methylation data

As described above, the prognostic significance of each CpG site is limited, and it would be more effective to combine the information from multiple CpG sites. One approach is an unsupervised analysis, including a cluster analysis, shown above. However, to construct a diagnostic system, supervised learning is more appropriate.

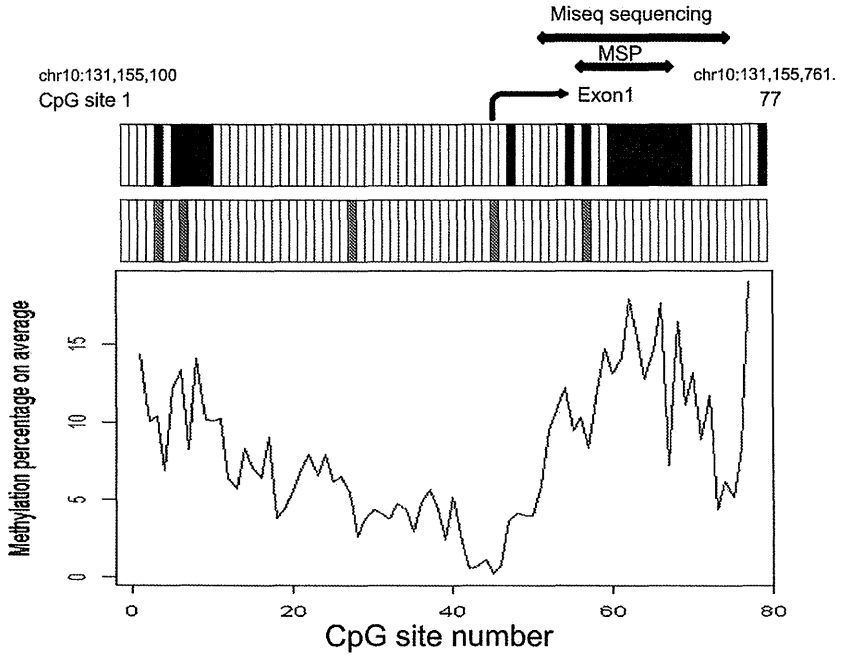

Figure 3 Proportion of methylation status and survival analysis at each CpG site. Average of the methylation percentage of CpG sites. The black and gray columns in the top panel indicate CpG sites with correlations with PFS and OS, respectively, that exceed the threshold ($p < 0.05$).

Here, based on the correlation between OS or PFS and the methylation status of the *MGMT* promoter region, we constructed a diagnostic system to predict the therapeutic outcomes of GB patients based on the methylation proportion of CpG51 - CpG74. Because we intended to use a next-generation sequencer for the validation study, we selected the CpG sites to be examined based on the read length restriction of the sequencer. This diagnostic score was denoted as the M-score (methylation score) and is defined as a weighted sum of the methylation proportion as follows:

$$M\_(methylation)\_score = -\sum_i A_i X_i$$

where 'A_i' is a regression coefficient deduced by univariate Cox analysis of PFS at CpG site i and 'X_i' is the methylation proportion at CpG site i. As described above, a correlation between OS and the methylation status was not clear in our patient population. We therefore used the same M-score calculation formula for OS as well. First, the performance of the M-score diagnostic system was evaluated by leave-one-out-cross-validation (LOOCV) using the 53 training samples. The 53 samples were divided into groups consisting of one and 52 samples, and 'Ai' was calculated by univariate Cox analysis using the data for the remaining 52 samples. The threshold was selected from M-scores of the 52 samples so that the log-rank p value of the Kaplan-Meier analysis for the two divided groups was minimized. In cases of multiple M-scores with the same minimum p value, the median was selected as the threshold. Next, the M-score of the one sample was calculated using parameters deduced from the 52 samples, and the sample was classified into either the good or poor prognosis group using the threshold. This process was repeated until all samples were tested. The LOOCV procedure is schematically shown in Additional file 1: Figure S2. The results of the LOOCV procedure are shown in Figure 4A and B; this approach demonstrated excellent prognostic ability with OS and PFS (OS, $p = 0.0381$; PFS, $p = 0.00122$). Thus, the diagnostic accuracy of our system is better than that of the MSP-based approach (Figure 4C, D) (OS, $p = 0.993$; PFS, $p = 0.113$).

Validation of the diagnostic system using next-generation sequencing

For validation of the test set, the parameters (Ai) were calculated using all 53 samples in the training set, and the threshold was set at 2.2, the average of the thresholds of the 53 LOOCV processes.

For the 32 test set samples, we performed qBGS with a next-generation sequencer, MiSeq, to examine the potential future applications of this approach. We also

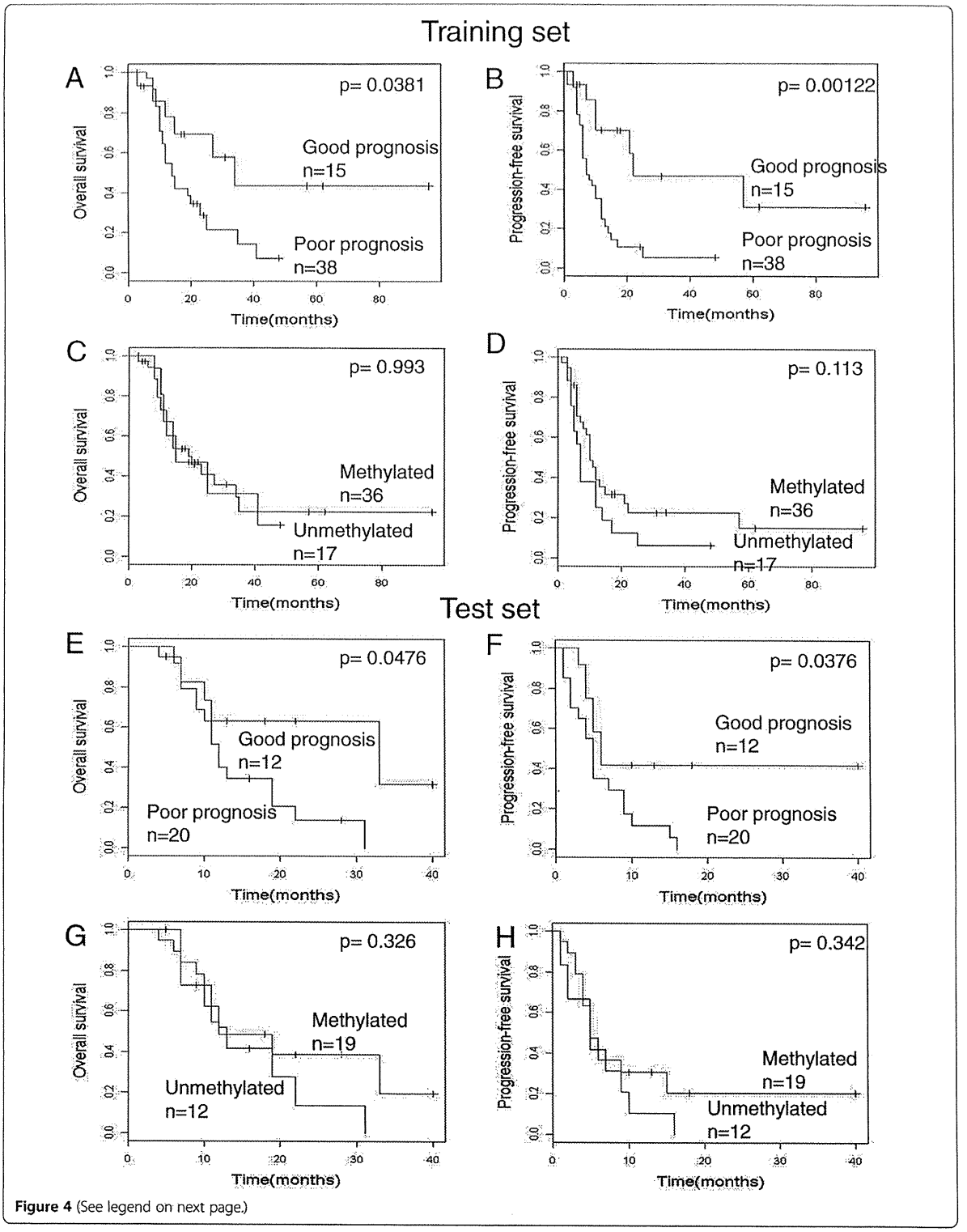

Figure 4 (See legend on next page.)

(See figure on previous page.)
Figure 4 Survival analysis of the training set by M-score and MSP. In each panel, the red line indicates either a good prognosis (M-score) or the methylated (MSP) group. The black line indicates either a poor prognosis (M-score) or the unmethylated (MSP) group. **(A)** training set, M-score, OS. **(B)** training set, M-score, PFS. **(C)** training set, MSP, OS. **(D)** training set, MSP, PFS. **(E)** test set, M-score, OS. **(F)** test set, M-score, PFS. **(G)** test set, MSP, OS. **(H)** test set, MSP, PFS.

performed MSP in all cases except one, due to the loss of genomic DNA. The mean depth of MiSeq sequencing was 80,817 reads. The methylation proportion of each CpG site was obtained, M-scores were calculated, and the test set samples were classified using the threshold listed above. Survival analysis indicated a statistically significant difference between the two groups with respect to PFS ($p = 0.0376$) and OS ($p = 0.0476$) (Figure 4E, F). There was no statistically significant difference between the two groups by classification with MSP (OS, $p = 0.326$; PFS, $p = 0.342$) (Figure 4G, H).

For potential future applications of this technique, we designed PCR primers that amplify the same region from FFPE samples. The method and results are shown in Additional file 4.

Multivariate Cox regression analysis

We performed Cox regression analysis to evaluate clinical parameters, such as age (above or below 60), gender, the extent of resection, post-operative chemotherapy (VAC-feron or TMZ), and the methylation status by the M-score sequencing method as predictors of OS and PFS in the GB patients in the test set. The variables with a p value < 0.2 were analyzed with a backward stepwise Multivariate Cox proportional hazard model. For OS, the best predictor was the M-score ($p = 0.0585$) (Hazard Ratio, 0.3558), and the next best prognostic factor was the extent of surgical resection ($p = 0.0739$) (Hazard Ratio, 0.5996). The M-score was found to be the best predictor of PFS ($p = 0.0247$; Hazard Ratio, 0.334).

Discussion

In this report, we characterized the methylation status of the entire *MGMT* promoter region using deep sequencing. The methylation status of each CpG site was quantitatively evaluated by sequencing multiple clones. Based on these results, we constructed a prognosis predictor that incorporates the methylation status of multiple CpG sites using supervised learning. The construction of a classifier using supervised learning is popular in the field of gene expression profiling, and we demonstrated here that the same approach is effective for the prediction of methylation status.

In our patient population, the correlation of the methylation status with OS was less clear than that with PFS. This is most likely due to variation of the therapy used after the first line therapy. The majority of our patients received repeated surgical resections, second line chemotherapy or additional radiotherapy. For multivariate analysis, age was not a prognosis factor, unlike in the past reports. We also performed surgical medical treatment with methylation-positive elderly patients. In particular, repeated surgery was likely to prolong the survival time of the glioblastoma patients with a poor prognosis.

MSP is the most widely used assay for methylation. However, MSP can only detect the CpG sites in the primer region; the methylation status of other CpG sites has no effect on the amplification. In a prior study, only 12.5% of the results obtained from two MSP experiments matched when the forward and reverse primers were different [35]. In addition, there is no established method to confirm the quality of bisulfite-converted genomic DNA. We assessed the quality using the Ct value of actin in real-time PCR. Approximately 64% of our glioma samples were methylation-positive with MSP. The positive rate was higher than that in other studies with some exceptions [36,37]. We excluded samples damaged by bisulfite treatment in the actin-based confirmation system, and this process may have increased the positive rate. This discrepancy in MSP results, which is most likely a false positive, might be influenced by the T genotype of the *MGMT* C > T (rs16906252) enhancer single-nucleotide polymorphism (SNP), which was reported by McDonald et al. [38] to interact with MGMT promotor methylation. Vlassenbroeck et al. also evaluated the results of qMSP based on the copy number of actin using real-time PCR [39]. It is often difficult to set a threshold for agarose gel patterns of MSP. This problem has been overcome by quantitative MSP [40,41]. Quantitative MSP was applied in two recent phase 3 trials of glioma [21,22]. However, the problem of limited coverage of CpG sites by MSP remains in need of technical improvements.

As discussed above, bisulfite sequencing can cover all CpG sites. In this context, pyrosequencing is considered to cover more CpG sites than MSP [26]. The methylation proportions can be semi-quantitatively deduced from the peak height of each incorporated nucleotide. The main disadvantage of pyrosequencing is its short read length [25,26]. qBGS using Sanger sequencing is not subject to this limitation, and its moderate read depth provides more accurate quantitative information. Because deep sequencing with the Sanger method is laborious, the use of next-generation sequencing may make this approach more comparable to pyrosequencing.

The major shortcoming of qBGS and pyrosequencing is the absence of a consensus regarding the data handling of multidimensional quantitative data. Dunn et al. and Motomura et al. used the average of the methylation proportion of multiple CpG sites (CpG51 - CpG62, Dunn et al.; CpG2 - CpG16, Motomura et al.) [42,43]. Karayan-Tapon et al. used the methylation proportion of five CpG sites (CpG 53–57) and grouped patients using the median value of the methylation proportion as the threshold [25]. We developed the M-score diagnostic system using the analysis method of gene expression profiling and calculated the optimized threshold by LOOCV. The M-score is the weighted sum of the methylation proportions of multiple CpG sites, which maximizes the correlation with the survival time. Our approach is more advanced than a simple summation of the population of methylated sites, and adding data from a larger patient population will improve the performance of the predictor. Bady et al. examined the quantitative value of 18 CpG sites in the *MGMT* promoter area using the Infinium methylation BeadChip and revealed two distinct CpG sites (CpG10 and CpG68). They converted multidimensional data to one methylation probability score using the inverse logit function. The classifier was validated with an external data set [44]. Both studies indicate a new direction for *MGMT* methylation assays based on evaluation of multiple CpG sites.

Shah et al. also quantitatively evaluated the methylation of the *MGMT* promoter [34]. Although the number of sequenced clones in that study was far less than that of our study (median of 10 clones), their results were similar to our results; the CpG sites located downstream of the transcription start site were often correlated with PFS. This prior study indicates that our observations are likely to be universal, and suggests that our prognosis predictor may be applicable to other patient populations.

The identification of biomarkers of gliomas has been an active area of research in recent years. It is well known that *IDH* mutations are a strong prognostic factor [45]. *IDH* mutations are associated with a hypermethylation phenotype [46], suggesting that the methylation of the *MGMT* promoter is one part of a genome-wide methylation profile [47]. Based on qBGS analysis, we identified different extents of methylation of CpG sites in the *MGMT* promoter region.

Recently, the methylation status of *MGMT* has become a focal point in the management of elderly GB patients. Two *MGMT* methylation analyses using samples from large phase 3 trials with elderly GB patients demonstrated that TMZ monotherapy was superior to conventional radiation therapy for the management of *MGMT*-methylated GB patients. Conversely, TMZ monotherapy was inferior to radiation therapy in GB cases with unmethylated *MGMT* [21,22]. These results indicate that the *MGMT* methylation status is a strong predictive factor for the efficacy of TMZ monotherapy in elderly GB patients and that evaluating *MGMT* methylation status is necessary for the management of these patients. The relationship between the efficacy of TMZ monotherapy and qBGS-based methylation analysis of the *MGMT* promoter in elderly GB merits further investigation.

In addition to its application for elderly patients, TMZ monotherapy has been utilized for low-grade glioma patients [20,48]. In this group, the co-deletion of 1p19q and *IDH* mutations were molecular prognostic factors. Given the findings in elderly GB patients, the methylation status of the *MGMT* promoter may also predict the outcomes of low-grade glioma patients treated by TMZ monotherapy. Because the *MGMT* promoter in normal tissue is generally unmethylated, methylated *MGMT* cases are susceptible to contamination by normal tissue. An advantage of qBGS is that it is easy to observe the state of contamination. qBGS also revealed intratumoral heterogeneity in the methylation of the *MGMT* promoter, which should be considered when using other methylation assays. Although qBGS is complicated and time-consuming, it is an important process for evaluating the methylation features of the *MGMT* promoter.

Conclusions

We constructed a novel diagnostic system to predict the prognosis of glioblastoma patients using information regarding the methylation status of the entire *MGMT* promoter region. A precise assessment of the methylation status of the *MGMT* promoter may improve the prediction of disease progression and assist in the choice of TMZ treatment.

Additional files

Additional file 1: Figure S1. Algorithm of quality assessment of bisulfite-treated genomic DNA. **Figure S2.** Schematic representation of leave-one-out cross-validation.

Additional file 2: Table S1. Table of regression coefficients of CpG sites based on PFS.

Additional file 3: Table S2. Table of regression coefficients of CpG sites based on OS.

Additional file 4: Agarose gel image of PCR product using FFPE genomic DNA.

Abbreviations

MGMT: O6-methylguanine-DNA methyltransferase; MSP: Methylation specific PCR, CpG, cytidine phosphate guanosine; PFS: Progression-free survival; OS: Overall survival; GB: Glioblastoma; TMZ: Temozolomide; qBGS: Quantitative bisulfite genome sequencing; DMSO: Dimethyl sulfoxide.

Competing interests

The authors declare that they have no competing interests.

Authors' contributions
MK, AN, KN and KT performed the experiments in this study. MS, YK, YA, SM and KK supervised the research. MK and KK wrote this manuscript. All authors approved the final manuscript.

Author details
[1]Research Institute, Osaka Medical Center for Cancer and Cardiovascular Diseases, 1-3-3 Nakamichi, Higashinari-ku, Osaka, Japan. [2]Department of Neurosurgery, Kyoto University Graduate School of Medicine, 54 Kawahara-cho, Shogoin, Sakyo-ku, Kyoto-shi, Kyoto 606-8507, Japan. [3]Department of Neuro-Oncology/Neurosurgery, Saitama Medical University International Medical Center, 1397-1 Yamane, Hidaka, Saitama 350-1298, Japan.

Received: 4 March 2014 Accepted: 27 August 2014
Published: 30 August 2014

References

1. Anderson E, Grant R, Lewis SC, Whittle IR: **Randomized Phase III controlled trials of therapy in malignant glioma: where are we after 40 years?** *Br J Neurosurg* 2008, **22**(3):339–349.
2. Stupp R, Mason WP, van den Bent MJ, Weller M, Fisher B, Taphoorn MJ, Belanger K, Brandes AA, Marosi C, Bogdahn U, Curschmann J, Janzer RC, Ludwin SK, Gorlia T, Allgeier A, Lacombe D, Cairncross JG, Eisenhauer E, Mirimanoff RO: **Radiotherapy plus concomitant and adjuvant temozolomide for glioblastoma.** *N Engl J Med* 2005, **352**(10):987–996.
3. Stupp R, Hegi ME, Mason WP, van den Bent MJ, Taphoorn MJ, Janzer RC, Ludwin SK, Allgeier A, Fisher B, Belanger K, Hau P, Brandes AA, Gijtenbeek J, Marosi C, Vecht CJ, Mokhtari K, Wesseling P, Villa S, Eisenhauer E, Gorlia T, Weller M, Lacombe D, Cairncross JG, Mirimanoff RO: **Effects of radiotherapy with concomitant and adjuvant temozolomide versus radiotherapy alone on survival in glioblastoma in a randomised phase III study: 5-year analysis of the EORTC-NCIC trial.** *Lancet Oncol* 2009, **10**(5):459–466.
4. Chinot OL, Wick W, Saran F, Mason WP, Henriksson R, Nishikawa R, Zeaiter AH, Moore N, Das A, Cloughesy TF: **AVAglio: a phase III trial of bevacizumab added to standard radiotherapy and temozolomide in patients with newly diagnosed glioblastoma.** *J Clin Oncol* 2011, **29**(suppl):abstr TPS136.
5. Friedman HS, Prados MD, Wen PY, Mikkelsen T, Schiff D, Abrey LE, Yung WK, Paleologos N, Nicholas MK, Jensen R, Vredenburgh J, Huang J, Zheng M, Cloughesy T: **Bevacizumab alone and in combination with irinotecan in recurrent glioblastoma.** *J Clin Oncol* 2009, **27**(28):4733–4740.
6. Gilbert MR, Dignam J, Won M, Blumenthal DT, Vogelbaum MA, Aldape KD, Colman H, Chakravarti A, Jeraj R, Armstrong TS, Wefel JS, Brown PD, Jaeckle KA, Schiff D, Atkins JN, Brachman D, Werner-Wasik M, Komaki R, Sulman EP, Mehta MP: **RTOG 0825: Phase III double-blind placebo-controlled trial evaluating bevacizumab (Bev) in patients (Pts) with newly diagnosed glioblastoma (GBM).** *J Clin Oncol* 2013, **31**(supp):abstr 1.
7. Drablos F, Feyzi E, Aas PA, Vaagbo CB, Kavli B, Bratlie MS, Pena-Diaz J, Otterlei M, Slupphaug G, Krokan HE: **Alkylation damage in DNA and RNA–repair mechanisms and medical significance.** *DNA Repair (Amst)* 2004, **3**(11):1389–1407.
8. Gerson SL: **MGMT: its role in cancer aetiology and cancer therapeutics.** *Nat Rev Cancer* 2004, **4**(4):296–307.
9. Kaina B, Christmann M, Naumann S, Roos WP: **MGMT: key node in the battle against genotoxicity, carcinogenicity and apoptosis induced by alkylating agents.** *DNA Repair (Amst)* 2007, **6**(8):1079–1099.
10. Nagarajan RP, Costello JF: **Epigenetic mechanisms in glioblastoma multiforme.** *Semin Cancer Biol* 2009, **19**(3):188–197.
11. Everhard S, Tost J, El Abdalaoui H, Criniere E, Busato F, Marie Y, Gut IG, Sanson M, Mokhtari K, Laigle-Donadey F, Hoang-Xuan K, Delattre JY, Thillet J: **Identification of regions correlating MGMT promoter methylation and gene expression in glioblastomas.** *Neuro Oncol* 2009, **11**(4):348–356.
12. Gerson SL: **Clinical relevance of MGMT in the treatment of cancer.** *J Clin Oncol* 2002, **20**(9):2388–2399.
13. Verbeek B, Southgate TD, Gilham DE, Margison GP: **O6-Methylguanine-DNA methyltransferase inactivation and chemotherapy.** *Br Med Bull* 2008, **85**:17–33.
14. Esteller M, Garcia-Foncillas J, Andion E, Goodman SN, Hidalgo OF, Vanaclocha V, Baylin SB, Herman JG: **Inactivation of the DNA-repair gene MGMT and the clinical response of gliomas to alkylating agents.** *N Engl J Med* 2000, **343**(19):1350–1354.
15. Gorlia T, van den Bent MJ, Hegi ME, Mirimanoff RO, Weller M, Cairncross JG, Eisenhauer E, Belanger K, Brandes AA, Allgeier A, Lacombe D, Stupp R: **Nomograms for predicting survival of patients with newly diagnosed glioblastoma: prognostic factor analysis of EORTC and NCIC trial 26981-22981/CE.3.** *Lancet Oncol* 2008, **9**(1):29–38.
16. Hegi ME, Diserens AC, Godard S, Dietrich PY, Regli L, Ostermann S, Otten P, Van Melle G, de Tribolet N, Stupp R: **Clinical trial substantiates the predictive value of O-6-methylguanine-DNA methyltransferase promoter methylation in glioblastoma patients treated with temozolomide.** *Clin Cancer Res* 2004, **10**(6):1871–1874.
17. Hegi ME, Diserens AC, Gorlia T, Hamou MF, de Tribolet N, Weller M, Kros JM, Hainfellner JA, Mason W, Mariani L, Bromberg JE, Hau P, Mirimanoff RO, Cairncross JG, Janzer RC, Stupp R: **MGMT gene silencing and benefit from temozolomide in glioblastoma.** *N Engl J Med* 2005, **352**(10):997–1003.
18. Hegi ME, Liu L, Herman JG, Stupp R, Wick W, Weller M, Mehta MP, Gilbert MR: **Correlation of O6-methylguanine methyltransferase (MGMT) promoter methylation with clinical outcomes in glioblastoma and clinical strategies to modulate MGMT activity.** *J Clin Oncol* 2008, **26**(25):4189–4199.
19. Gallego Perez-Larraya J, Ducray F, Chinot O, Catry-Thomas I, Taillandier L, Guillamo JS, Campello C, Monjour A, Cartalat-Carel S, Barrie M, Huchet A, Beauchesne P, Matta M, Mokhtari K, Tanguy ML, Honnorat J, Delattre JY: **Temozolomide in elderly patients with newly diagnosed glioblastoma and poor performance status: an ANOCEF phase II trial.** *J Clin Oncol* 2011, **29**(22):3050–3055.
20. Taal W, Dubbink HJ, Zonnenberg CB, Zonnenberg BA, Postma TJ, Gijtenbeek JM, Boogerd W, Groenendijk FH, Kros JM, Kouwenhoven MC, van Marion R, van Heuvel I, van der Holt B, Bromberg JE, Sillevis Smitt PA, Dinjens WN, van den Bent MJ: **First-line temozolomide chemotherapy in progressive low-grade astrocytomas after radiotherapy: molecular characteristics in relation to response.** *Neuro Oncol* 2011, **13**(2):235–241.
21. Malmstrom A, Gronberg BH, Marosi C, Stupp R, Frappaz D, Schultz H, Abacioglu U, Tavelin B, Lhermitte B, Hegi ME, Rosell J, Henriksson R: **Temozolomide versus standard 6-week radiotherapy versus hypofractionated radiotherapy in patients older than 60 years with glioblastoma: the Nordic randomised, phase 3 trial.** *Lancet Oncol* 2012, **13**(9):916–926.
22. Wick W, Platten M, Meisner C, Felsberg J, Tabatabai G, Simon M, Nikkhah G, Papsdorf K, Steinbach JP, Sabel M, Combs SE, Vesper J, Braun C, Meixensberger J, Ketter R, Mayer-Steinacker R, Reifenberger G, Weller M: **Temozolomide chemotherapy alone versus radiotherapy alone for malignant astrocytoma in the elderly: the NOA-08 randomised, phase 3 trial.** *Lancet Oncol* 2012, **13**(7):707–715.
23. Parkinson JF, Wheeler HR, Clarkson A, McKenzie CA, Biggs MT, Little NS, Cook RJ, Messina M, Robinson BG, McDonald KL: **Variation of O(6)-methylguanine-DNA methyltransferase (MGMT) promoter methylation in serial samples in glioblastoma.** *J Neurooncol* 2008, **87**(1):71–78.
24. Rand K, Qu W, Ho T, Clark SJ, Molloy P: **Conversion-specific detection of DNA methylation using real-time polymerase chain reaction (ConLight-MSP) to avoid false positives.** *Methods* 2002, **27**(2):114–120.
25. Karayan-Tapon L, Quillien V, Guilhot J, Wager M, Fromont G, Saikali S, Etcheverry A, Hamlat A, Loussouarn D, Campion L, Campone M, Vallette FM, Gratas-Rabbia-Re C: **Prognostic value of O6-methylguanine-DNA methyltransferase status in glioblastoma patients, assessed by five different methods.** *J Neurooncol* 2010, **97**(3):311–322.
26. Mikeska T, Bock C, El-Maarri O, Hubner A, Ehrentraut D, Schramm J, Felsberg J, Kahl P, Buttner R, Pietsch T, Waha A: **Optimization of quantitative MGMT promoter methylation analysis using pyrosequencing and combined bisulfite restriction analysis.** *J Mol Diagn* 2007, **9**(3):368–381.
27. Aoki T, Takahashi JA, Ueba T, Oya N, Hiraoka M, Matsui K, Fukui T, Nakashima Y, Ishikawa M, Hashimoto N: **Phase II study of nimustine, carboplatin, vincristine, and interferon-beta with radiotherapy for glioblastoma multiforme: experience of the Kyoto Neuro-Oncology Group.** *J Neurosurg* 2006, **105**(3):385–391.
28. Shirahata M, Iwao-Koizumi K, Saito S, Ueno N, Oda M, Hashimoto N, Takahashi JA, Kato K: **Gene expression-based molecular diagnostic system for malignant gliomas is superior to histological diagnosis.** *Clin Cancer Res* 2007, **13**(24):7341–7356.
29. Shirahata M, Oba S, Iwao-Koizumi K, Saito S, Ueno N, Oda M, Hashimoto N, Ishii S, Takahashi JA, Kato K: **Using gene expression profiling to identify a prognostic molecular spectrum in gliomas.** *Cancer Sci* 2009, **100**(1):165–172.

30. Reesink-Peters N, Wisman GB, Jeronimo C, Tokumaru CY, Cohen Y, Dong SM, Klip HG, Buikema HJ, Suurmeijer AJ, Hollema H, Boezen HM, Sidransky D, van der Zee AG: **Detecting cervical cancer by quantitative promoter hypermethylation assay on cervical scrapings: a feasibility study.** *Mol Cancer Res* 2004, 2(5):289–295.
31. Esteller M, Hamilton SR, Burger PC, Baylin SB, Herman JG: **Inactivation of the DNA repair gene O6-methylguanine-DNA methyltransferase by promoter hypermethylation is a common event in primary human neoplasia.** *Cancer Res* 1999, 59(4):793–797.
32. Li H, Durbin R: **Fast and accurate short read alignment with Burrows-Wheeler transform.** *Bioinformatics* 2009, 25(14):1754–1760.
33. Li H, Handsaker B, Wysoker A, Fennell T, Ruan J, Homer N, Marth G, Abecasis G, Durbin R: **The Sequence Alignment/Map format and SAMtools.** *Bioinformatics* 2009, 25(16):2078–2079.
34. Shah N, Lin B, Sibenaller Z, Ryken T, Lee H, Yoon JG, Rostad S, Foltz G: **Comprehensive analysis of MGMT promoter methylation: correlation with MGMT expression and clinical response in GBM.** *PLoS One* 2011, 6(1):e16146.
35. van Nifterik KA, van den Berg J, van der Meide WF, Ameziane N, Wedekind LE, Steenbergen RD, Leenstra S, Lafleur MV, Slotman BJ, Stalpers LJ, Sminia P: **Absence of the MGMT protein as well as methylation of the MGMT promoter predict the sensitivity for temozolomide.** *Br J Cancer* 2010, 103(1):29–35.
36. Gerstner ER, Yip S, Wang DL, Louis DN, Iafrate AJ, Batchelor TT: **Mgmt methylation is a prognostic biomarker in elderly patients with newly diagnosed glioblastoma.** *Neurology* 2009, 73(18):1509–1510.
37. Reifenberger G, Hentschel B, Felsberg J, Schackert G, Simon M, Schnell O, Westphal M, Wick W, Pietsch T, Loeffler M, Weller M: **Predictive impact of MGMT promoter methylation in glioblastoma of the elderly.** *Int J Cancer* 2012, 131(6):1342–1350.
38. McDonald KL, Rapkins RW, Olivier J, Zhao L, Nozue K, Lu D, Tiwari S, Kuroiwa-Trzmielina J, Brewer J, Wheeler HR, Hitchins MP: **The T genotype of the MGMT C > T (rs16906252) enhancer single-nucleotide polymorphism (SNP) is associated with promoter methylation and longer survival in glioblastoma patients.** *Eur J Cancer* 2013, 49(2):360–368.
39. Vlassenbroeck I, Califice S, Diserens AC, Migliavacca E, Straub J, Di Stefano I, Moreau F, Hamou MF, Renard I, Delorenzi M, Flamion B, DiGuiseppi J, Bierau K, Hegi ME: **Validation of real-time methylation-specific PCR to determine O6-methylguanine-DNA methyltransferase gene promoter methylation in glioma.** *J Mol Diagn* 2008, 10(4):332–337.
40. Hattermann K, Mehdorn HM, Mentlein R, Schultka S, Held-Feindt J: **A methylation-specific and SYBR-green-based quantitative polymerase chain reaction technique for O6-methylguanine DNA methyltransferase promoter methylation analysis.** *Anal Biochem* 2008, 377(1):62–71.
41. Metellus P, Coulibaly B, Nanni I, Fina F, Eudes N, Giorgi R, Barrie M, Chinot O, Fuentes S, Dufour H, Ouafik L, Figarella-Branger D: **Prognostic impact of O6-methylguanine-DNA methyltransferase silencing in patients with recurrent glioblastoma multiforme who undergo surgery and carmustine wafer implantation: a prospective patient cohort.** *Cancer* 2009, 115(20):4783–4794.
42. Dunn J, Baborie A, Alam F, Joyce K, Moxham M, Sibson R, Crooks D, Husband D, Shenoy A, Brodbelt A, Wong H, Liloglou T, Haylock B, Walker C: **Extent of MGMT promoter methylation correlates with outcome in glioblastomas given temozolomide and radiotherapy.** *Br J Cancer* 2009, 101(1):124–131.
43. Motomura K, Natsume A, Kishida Y, Higashi H, Kondo Y, Nakasu Y, Abe T, Namba H, Wakai K, Wakabayashi T: **Benefits of interferon-beta and temozolomide combination therapy for newly diagnosed primary glioblastoma with the unmethylated MGMT promoter: A multicenter study.** *Cancer* 2011, 117(8):1721–1730.
44. Bady P, Sciuscio D, Diserens AC, Bloch J, van den Bent MJ, Marosi C, Dietrich PY, Weller M, Mariani L, Heppner FL, McDonald DR, Lacombe D, Stupp R, Delorenzi M, Hegi ME: **MGMT methylation analysis of glioblastoma on the Infinium methylation BeadChip identifies two distinct CpG regions associated with gene silencing and outcome, yielding a prediction model for comparisons across datasets, tumor grades, and CIMP-status.** *Acta Neuropathol* 2012, 124(4):547–560.
45. Yan H, Parsons DW, Jin G, McLendon R, Rasheed BA, Yuan W, Kos I, Batinic-Haberle I, Jones S, Riggins GJ, Friedman H, Friedman A, Reardon D, Herndon J, Kinzler KW, Velculescu VE, Vogelstein B, Bigner DD: **IDH1 and IDH2 mutations in gliomas.** *N Engl J Med* 2009, 360(8):765–773.
46. Noushmehr H, Weisenberger DJ, Diefes K, Phillips HS, Pujara K, Berman BP, Pan F, Pelloski CE, Sulman EP, Bhat KP, Verhaak RG, Hoadley KA, Hayes DN, Perou CM, Schmidt HK, Ding L, Wilson RK, Van Den Berg D, Shen H, Bengtsson H, Neuvial P, Cope LM, Buckley J, Herman JG, Baylin SB, Laird PW, Aldape K: **Identification of a CpG island methylator phenotype that defines a distinct subgroup of glioma.** *Cancer Cell* 2010, 17(5):510–522.
47. van den Bent MJ, Gravendeel LA, Gorlia T, Kros JM, Lapre L, Wesseling P, Teepen JL, Idbaih A, Sanson M, Smitt PA, French PJ: **A hypermethylated phenotype is a better predictor of survival than MGMT methylation in anaplastic oligodendroglial brain tumors: a report from EORTC study 26951.** *Clin Cancer Res* 2011, 17(22):7148–7155.
48. Hoang-Xuan K, Capelle L, Kujas M, Taillibert S, Duffau H, Lejeune J, Polivka M, Criniere E, Marie Y, Mokhtari K, Carpentier AF, Laigle F, Simon JM, Cornu P, Broet P, Sanson M, Delattre JY: **Temozolomide as initial treatment for adults with low-grade oligodendrogliomas or oligoastrocytomas and correlation with chromosome 1p deletions.** *J Clin Oncol* 2004, 22(15):3133–3138.

doi:10.1186/1471-2407-14-641
Cite this article as: Kanemoto *et al.*: Prognostic prediction of glioblastoma by quantitative assessment of the methylation status of the entire *MGMT* promoter region. *BMC Cancer* 2014 14:641.

Neuroradiology (2014) 56:297–303
DOI 10.1007/s00234-014-1334-2

DIAGNOSTIC NEURORADIOLOGY

Quantitative imaging values of CT, MR, and FDG-PET to differentiate pineal parenchymal tumors and germinomas: are they useful?

Takahide Kakigi · Tomohisa Okada · Mitsunori Kanagaki · Akira Yamamoto · Yasutaka Fushimi · Ryo Sakamoto · Yoshiki Arakawa · Yoshiki Mikami · Taro Shimono · Jun C. Takahashi · Kaori Togashi

Received: 26 November 2013 / Accepted: 22 January 2014 / Published online: 9 February 2014

Abstract
Introduction Quantitative values of CT attenuation, apparent diffusion coefficient (ADC), and standardized uptake value (SUV) were investigated for differentiation between pineal parenchymal tumors (PPTs) and germinomas. Differences in age, sex, and calcification pattern were also evaluated.
Methods Twenty-three patients with PPTs and germinomas in 20 years were retrospectively enrolled under the approval of the institutional review board. CT attenuation, ADC, and SUV (20, 13, and 10 patients, respectively) were statistically compared between the two tumors. Differences in sex and patterns of calcification ("exploded" or "engulfed") were also examined. Mean patient ages were compared among three groups of pineoblastoma, pineal parenchymal tumor of intermediate differentiation, (PPTID) and pineocytoma and germinoma.
Results None of the quantitative values of CT attenuation, ADC, and SUV showed significant differences between PPTs and germinomas ($p>.05$). However, there was a significant difference in age ($p<.05$) among the three groups of pineoblastoma (mean age ± standard deviation 7.0±8.7 years), PPTID, and pineocytoma (53.7±11.4 years) and germinoma (19.1±8.1 years). Sex also showed significant differences between PPTs and germinomas ($p=.039$). Exploded pattern of calcification was found in 9 of 11 PPT patients and engulfed pattern in 7 of 9 patients with germinomas. No reverse pattern was observed, and the patterns of calcification were considered highly specific of tumor types.
Conclusions None of the quantitative imaging values could differentiate PPTs from germinomas. Age, sex, and calcification patterns were confirmed useful in differentiating these tumors to some degree.

Keywords Pineal tumor · Germinoma · CT attenuation · Apparent diffusion coefficient · Standardized uptake value

T. Kakigi · T. Okada (✉) · M. Kanagaki · A. Yamamoto · Y. Fushimi · R. Sakamoto · K. Togashi
Department of Diagnostic Imaging and Nuclear Medicine, Kyoto University Graduate School of Medicine, 54 Shogoin Kawahara-cho, Sakyo-ku, Kyoto 606-8507, Japan
e-mail: tomokada@kuhp.kyoto-u.ac.jp

Y. Arakawa · J. C. Takahashi
Department of Neurosurgery, Kyoto University Graduate School of Medicine, Kyoto, Japan

Y. Mikami
Department of Pathology, Kyoto University Graduate School of Medicine, Kyoto, Japan

T. Shimono
Department of Radiology, Osaka City University Graduate School of Medicine, Osaka, Japan

Introduction

Tumors of the pineal region are uncommon and account for approximately 0.4–1 % of all intracranial tumors in American and European literatures, but higher incidence of up to 3.2 % is reported from Japan [1]. Pineal tumors consist of a very heterogeneous group of tumors including germ cell tumors (GCTs) (40 %), pineal parenchymal tumors (PPTs) (14–27 %), and neuroepithelial tumors, such as astrocytoma, ependymoma, and papillary tumor of the pineal region [1–3]. In GCTs, germinoma accounts for the majority of intracranial GCTs (68–86 %) [2, 4, 5], which can be treated successfully with a combination of chemotherapy and radiotherapy. Therefore, biopsy is sufficient for the diagnosis of germinoma [6], which is different from PPTs that are categorized into three subtypes: pineocytoma (grade 1), pineal

parenchymal tumor of intermediate differentiation (PPTID) (grade 2 or 3), and pineoblastoma (grade 4) [3, 7]. Surgical resection is mainly selected for pineocytoma occasionally combined with adjuvant chemotherapy and/or radiotherapy [8]. Treatment of PPTID varies from surgery to radiotherapy (radiosurgery or craniospinal irradiation) alone and chemotherapy [9, 10]. Standard care of pineoblastoma includes maximal surgical resection with adjuvant craniospinal radiation and systemic chemotherapy [11]. Therefore, the differentiation between germinoma and PPTs before surgical procedure is highly important.

For the differentiation between PPTs and germinomas, age, sex, and patterns of calcification, i.e., "exploded" or "engulfed", have been reported useful [2, 4, 12], and physiological pineal calcifications are frequently observed on CT [13].Other imaging characteristics of these tumors at the pineal region have been described on CT and MRI, but their qualitative evaluations could not differentiate the two entities [14, 15]. However, there have been only few studies on ^{18}F-fluoro-2-deoxy-D-glucose-positron emission tomography (FDG-PET). There were only two case reports on FDG-PET findings in pineoblastoma [16] and mixed GCT [17]. No comprehensive imaging study including all conventional imaging methods of CT, MRI, and FDG-PET has been conducted to differentiate germinomas and PPTs.

The purpose of this study was to make a comprehensive evaluation on differential capability between germinomas and PPTs using the quantitative values of CT attenuation, apparent diffusion coefficient (ADC), and standardized uptake value (SUV). We also evaluated their age, sex, and patterns of calcification as exploded or engulfed, if calcification was present on CT.

Materials and methods

Patients

This study was approved by the institutional review board. Informed consent was waived due to retrospective nature of this study. The institutional medical recording system and the pathology database were searched for patients who had CT, MR, and FDG-PET imaging with histological verification of germinoma and PPTs between January 1993 and December 2012. Twenty-three patient records (12 female and 11 male subjects; mean 31 years old, ranged from 1 to 68 years) were found and analyzed for this study. Twelve patients had PPTs (five pineocytomas, four PPTIDs, and three pineoblastomas), and 11 patients had pure germinomas. Imaging was conducted using CT, MRI, and FDG-PET in 23, 14, and 10 patients, respectively, but three and one patients were excluded from CT and MRI, respectively, because they were scanned after biopsy. Patient characteristics are summarized in Table 1.

CT imaging

CT images were obtained with a 64-channel multi-detector row CT (MDCT) scanner for 5 patients, a 16-channel MDCT scanner for 4 patients (Aquilion 64 and 16, respectively, Toshiba Medical Systems, Otawara, Japan), and a 4-channel MDCT scanner for 11 patients (W-3000, Hitachi Medical Co., Tokyo, Japan). Resolutions of all the CT images were 0.4×0.4×7–8 mm.

MR imaging

MR scans were conducted with a 3T scanner for six patients and a 1.5T scanner for five patients (MAGNETOM Trio and MAGNETOM Symphony, respectively, Siemens Medical Systems, Erlangen, Germany). The other 1.5T scanner was used for two patients (Signa Genesis, GE Medical Systems, Milwaukee, WI, USA). In addition to axial T1-weighted, T2-weighted, and FLAIR images, contrast-enhanced axial T1-weighted images were acquired after the administration of a Gadolinium contrast agent (0.1 mmol/kg). Diffusion-weighted imaging (DWI) was acquired with the following parameters: TR=3,700–10,000 ms; TE=80–101 ms; slice thickness=3–5 mm; slice spacing=1–1.8 mm; pixel spacing=0.9–1.7 mm×0.9–1.7 mm; FOV=220×220 mm. DWI was conducted with two different motion-probing gradient values (b=0 and 1,000 s/mm^2) applied in three orthogonal directions. The acquired images were combined to form a single composite DWI, and their ADC values were calculated for each pixel to make ADC images.

FDG-PET imaging

FDG-PET scans were conducted using a PET/CT scanner for seven patients and a PET scanner for three patients (Discovery ST Elite and Advance, respectively, GE Healthcare, Waukesha, WI, USA). Patients fasted for at least 4 h prior to the scans. After intravenous administration of 4 MBq/kg of FDG, the patients rested in a waiting room for 30 min. Emission scans of the brain were conducted for 15 min with 128×128 matrix and 47 slices and 128×128 matrix and 35 slices, resulting in resolutions of 2.0×2.0×3.27 mm and 2.0×2.0×4.25 mm, respectively, for the scanners.

Data analysis

All images were evaluated independently by two experienced neuroradiologists (T.K. and R.S., both had experience in diagnostic imaging for 9 years) blinded to clinical data. Region of interests (ROIs) for the tumors were defined on an analysis console (Advantage Workstation 4.4, GE Medical Systems, Milwaukee, WI, USA) to measure maximum and mean nonenhanced CT attenuation values (CTmax and CTmean,

Table 1 Patient characteristics and quantitative imaging values

No.	Age	Sex	Pathology	CTmean (HU)	CTmax (HU)	Calcification	ADCmean ($\times 10^{-6}$ mm^2/s)	ADCmin ($\times 10^{-6}$ mm^2/s)	SUVmean	SUVmax
1	55	F	Pineocytoma	33.8	48.5	Exploded	912.3	606.5	5.1	7.72
2	63	F	Pineocytoma	40.6	54	–	813.2	570	NA	NA
3	62	F	Pineocytoma	36.2	48	Exploded	523.1	391	16.82	28.82
4	30	M	Pineocytoma	36.1	47.5	Exploded	653.1	488.5	9.39	11.76
5	68	M	Pineocytoma	39	58.5	Exploded	747.2	574	5.59	6.67
6	55	F	PPTID	39.3	57	Exploded	NA	NA	NA	NA
7	55	F	PPTID	32.8	48	Exploded	1,406.4	1,160	5.53	6.26
8	43	F	PPTID	39.8	57	–	NA	NA	NA	NA
9	52	F	PPTID	40.4	53	Exploded	996.1	705	NA	NA
10	17	F	Pineoblastoma	45	58	Exploded	NA	NA	NA	NA
11	1	F	Pineoblastoma	43.4	67	Exploded	750.1	321.3	NA	NA
12	3	M	Pineoblastoma	NA	NA	NA	NA	NA	5.87	6.43
1	8	F	Germinoma	40.4	53	–	NA	NA	NA	NA
2	8	F	Germinoma	40	55.5	–	NA	NA	NA	NA
3	22	M	Germinoma	43.6	57.5	Engulfed	NA	NA	NA	NA
4	33	M	Germinoma	45.1	59.5	Engulfed	813.6	321.3	NA	NA
5	14	M	Germinoma	NA	NA	NA	758.6	550	NA	NA
6	21	M	Germinoma	49.5	62	Engulfed	NA	NA	NA	NA
7	26	M	Germinoma	NA	NA	NA	NA	NA	5.43	9.4
8	22	M	Germinoma	37.1	52	Engulfed	639.5	414	8.26	9.88
9	17	M	Germinoma	41.2	64	Engulfed	NA	NA	9.05	12.42
10	12	F	Germinoma	39.4	53.5	Engulfed	825.7	325	2.74	3.58
11	27	M	Germinoma	40	60	Engulfed	725.4	470	NA	NA

ADC apparent diffusion coefficient, *HU* Hounsfield unit, *NA* not available, *PPTID* pineal parenchymal tumor of intermediate differentiation, *SUV* standardized uptake value

respectively), mean and minimum ADC values (ADCmean and ADCmin, respectively), and mean and maximum SUV (SUVmean and SUVmax, respectively). ROIs were drawn on one slice with the largest enhancement area by referring to the MR or CT images. Regions suggestive of a cystic change, necrosis, or calcification were excluded from the ROIs. When only FDG-PET imaging existed (one patient of pineoblastoma and one patient of germinoma), ROIs were drawn by referring to FDG uptakes. We evaluated the presence and the pattern of calcification as exploded or engulfed on axial nonenhanced CT.

Statistical analysis

Interobserver variability was evaluated using intraclass correlation coefficient (ICC) [18] for measuring the quantitative values and ROI sizes. The measured values obtained by the two evaluators were averaged and compared between germinoma and PPTs using the Mann-Whitney test. Age difference was compared among the three groups of germinomas, pineoblastomas, and PPTIDs and pineocytomas using Kruskal-Wallis test because the pineoblastoma is found in much younger patients than the pineocytoma or PPTID. Sex difference was examined with Fisher's exact test. A p value less than .05 was considered statistically significant. Statistical analysis was conducted with a commercially available statistical software package (MedCalc version 12.5.0, MedCalc software, Mariakerke, Belgium).

Results

ICCs were 0.76 to 0.99, which were recognized as good to excellent interobserver reproducibility [19] for all the quantitative values and ROI sizes. Statistically significant difference was not found between germinoma and PPTs for any of the measured quantitative values (p=.17, .08, .72, .09, .61, and .91, respectively, for CTmax, CTmean, ADCmean, ADCmin, SUVmean, and SUVmax; see Tables 1 and 2 and Figs. 1, 2, 3, and 4).

Calcification was detected in 9 of 12 patients (75 %) with PPTs, and all cases showed exploded calcification. Seven of 11 patients with germinoma had calcification, and engulfed calcification was found in all cases (Fig. 4). No discrepancy was observed between the observers.

The mean ages ± standard deviations were 19.1±8.1, 7.0± 8.7, and 53.7±11.4 years old for patients with germinoma,

Table 2 Differences between PPT and germinoma in CTmax, CTmean, ADCmean, ADCmin, SUVmean, and SUVmax

Quantitative values	*n*	PPT Median (interquartile range)	G Median (interquartile range)	*p* value
CTmax (HU)	20	54.0 (48.1–57.8)	57.5 (53.4–60.5)	.17
CTmean (HU)	20	39.3 (36.1–40.6)	40.4 (39.8–44.0)	.08
ADCmean ($\times 10^{-6}$ mm^2/s)	13	781.6 (700.1–954.2)	758.6 (703.9–816.6)	.72
ADCmin ($\times 10^{-6}$ mm^2/s)	13	572.0 (439.8–655.8)	414.0 (324.1–490.0)	.09
SUVmean	10	5.73 (5.53–9.39)	6.85 (4.09–8.66)	.61
SUVmax	10	7.20 (6.43–11.76)	9.64 (6.49–11.15)	.91

ADC apparent diffusion coefficient, *G* germinoma, *HU* Hounsfield unit, *PPT* pineal parenchymal tumor, *SUV* standardized uptake value

pineoblastoma, and PPTIDs and pineocytomas, respectively. When these three groups were compared, significant difference was observed among all the three groups ($p<.05$, post hoc analysis, Fig. 5). Eight out of 11 patients were male in germinoma, and 9 out of 12 were female in PPTs. The difference was statistically significant ($p=.039$).

Discussion

This is the first study that investigated quantitative imaging values of CT attenuation, ADC, and SUV, comprehensively, for differentiation between germinomas and PPTs. The imaging spectrum of these tumors has been described [2, 4, 12, 14, 15], but most findings are limited to CT or MRI. There are two case reports on its very high uptake by FDG-PET imaging in pineoblastoma [16] and little uptake in mixed GCT [17], but no report exists on pineocytoma and PPTID on FDG-PET. Moreover, no comparison has been conducted comprehensive of all modalities between PPT and germinoma, which was conducted in this study. We focused on pure germinoma because GCTs except germinoma can be generally differentiated using serum and cerebrospinal fluid (CSF) levels of tumor-produced oncoproteins (α-fetoprotein, β-human chorionic gonadotropin (β-hCG), and placental alkaline phosphatase) [2].

On CT, the pineoblastoma and germinoma are frequently recognized as hyperattenuating masses, which reflect highly cellular histologic features compared with the pineocytoma and PPTID [2]. However, the difference in the CT value between the germinoma and PPT was around 3 Hounsfield unit (HU) (see Table 2), which was not statistically significant.

Dumrongpisutikul et al. [20] have proposed the utility of ADC values between the germinoma and PPT. They found that germinoma had higher ADC values than the pineal cell tumors; however, we found no significant difference in ADC values between PPTs and germinoma. They drew the ROIs covering the entire lesions inclusive of cystic or necrotic regions, while we put them on areas with contrast enhancement because such region size may vary. The ADC value of the solid portion of the tumor is considered to have limited role in making differential diagnosis.

In FDG-PET, no study that compared between PPTs and germinomas has been reported. This is the first study to investigate the difference, but no significant difference was found

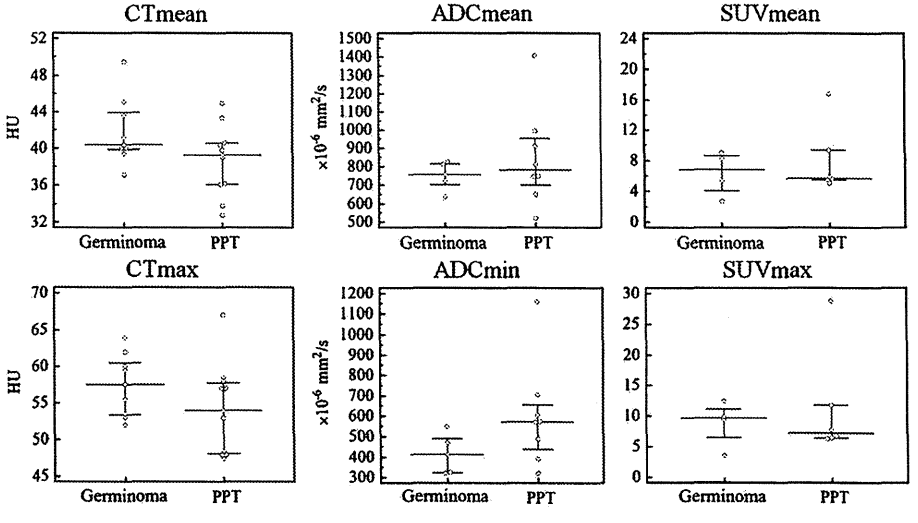

Fig. 1 Plots of quantitative values for comparisons between PPT and germinoma. No significant difference was observed between them. The *long horizontal bars* indicate median values, and the *short horizontal bars* show interquartile range. *ADC* apparent diffusion coefficient, *HU* Hounsfield unit, *PPT* pineal parenchymal tumor, *SUV* standardized uptake value

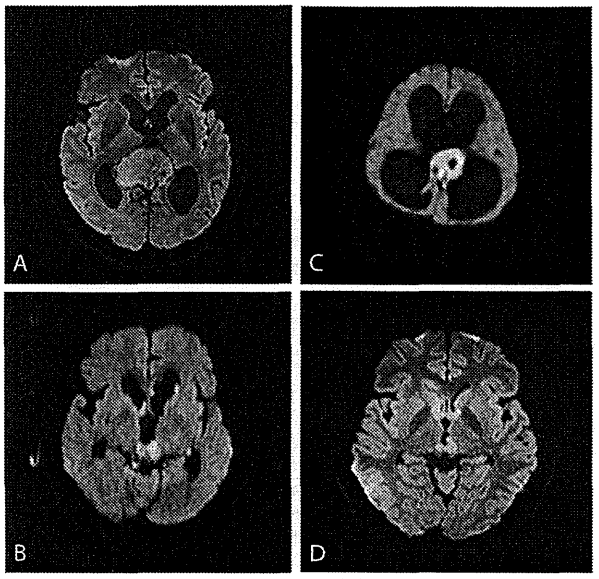

Fig. 2 Diffusion-weighted images of pathologically proven **a** pineocytoma, **b** PPTID, **c** pineoblastoma, and **d** germinoma. They have minimum ADC values of 574, 705, 343, and 325×10^{-6} mm^2/s, respectively. *ADC* apparent diffusion coefficient, *PPTID* pineal parenchymal tumor of intermediate differentiation

between germinomas and PPTs. In average, germinomas had higher SUVs than PPTs, although two cases of pineocytoma had very high SUVs (see Table 1).The pineocytoma is a low-grade tumor and may retain functionality. FDG uptake reflects not only cell density and mitotic activity of pineal tumors but also other activities such as regulation of certain circulating

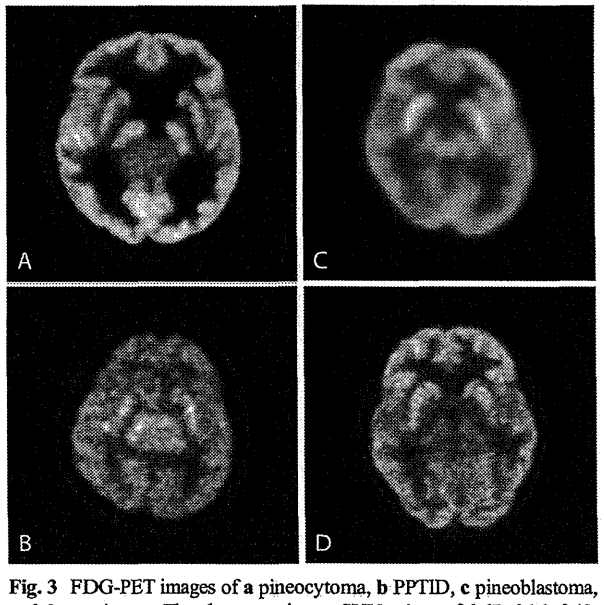

Fig. 3 FDG-PET images of **a** pineocytoma, **b** PPTID, **c** pineoblastoma, and **d** germinoma. They have maximum SUV values of 6.67, 6.26, 6.43, and 9.88, respectively. *PPTID* pineal parenchymal tumor of intermediate differentiation, *SUV* standardized uptake value

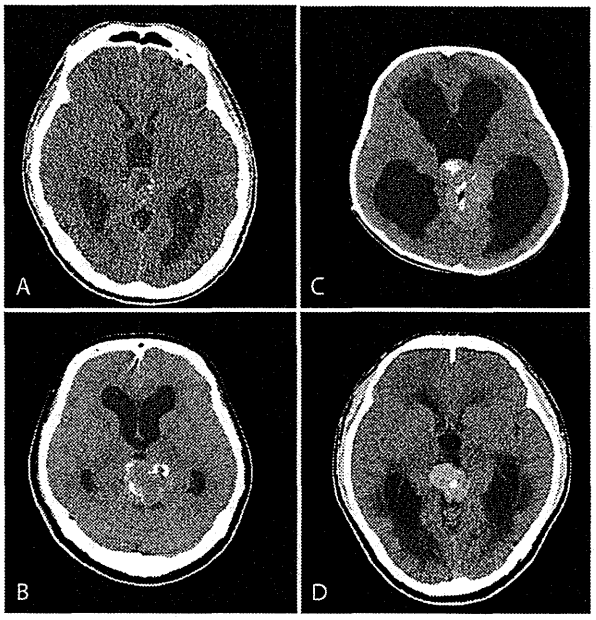

Fig. 4 CT images of pathologically proven **a** pineocytoma, **b** PPTID, **c** pineoblastoma, and **d** germinoma. They have mean CT values of 36.1, 32.8, 45.0, and 49.5 HU, respectively. Cases **a**, **b**, and **c** show "exploded" calcfication, whereas case **d** shows "engulfed" calcification. *HU* Hounsfield unit, *PPTID* pineal parenchymal tumor of intermediate differentiation

hormone levels and short-term (e.g., diurnal or circadian) biologic rhythm [13]. Such complex activity of the pineal tumor may result in failure of differentiation using SUV values.

It has already been reported that germinomas "engulf" physiological calcifications, whereas PPTs scatter or "explode" calcifications [2, 4]. When calcification existed, the

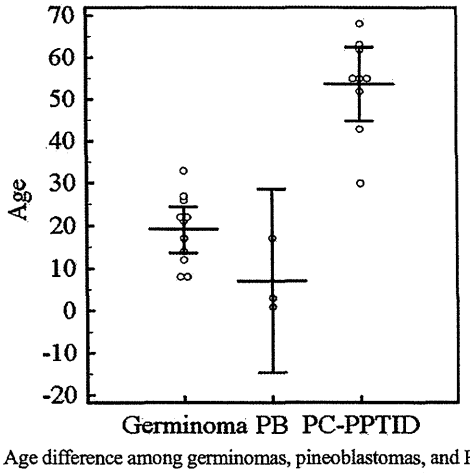

Fig. 5 Age difference among germinomas, pineoblastomas, and PPTIDs and pineocytomas. Significant differences observed in all pairs of the three groups ($p<.05$, *post hoc* analysis). The *long horizontal bars* indicate mean values, and the *short horizontal bars* show 95 % confidence intervals. *PB* pineoblastoma, *PC* pineocytoma, *PPTID* pineal parenchymal tumor of intermediate differentiation

pattern classification was considered to have high differentiation capability of the two. In this study, these two tumors were completely differentiated by the patterns with no disagreement between the two evaluators. However, calcification was detected in 75 % on nonenhanced CT. Other clues for differentiation might be required.

The pineocytoma and PPTID occur predominantly in adults from the third to sixth decades of age [13], whereas the pineoblastoma most commonly occurs in the first two decades [7].Ninety percent of patients with germinoma are less than 20 years old [4, 7]. The mean ages of the three tumor groups were statistically significant, but there was a large overlap between pineoblastoma and germinoma (see Fig. 5), and the differentiation was considered difficult between them.

No gender predilection is reported in pineocytoma and pineoblastoma, but a slight female preponderance is reported in PPTID [2, 7]. Germinoma in the pineal region are 10 times more common in men [7]. In this study, all of the PPTID patients were female, and male predominance was found in germinoma. Statistically, there was a significant difference between PPT and germinoma in sex. However, there were three female patients out of 11 germinoma patients, and its differentiation from pineoblastoma is considered difficult.

There is a limitation in this retrospective study that the numbers of patients with PPTs and germinomas were relatively small, which is inevitable considering the relative rarity of these tumors. As the other limitation, we have to consider errors caused by the difference in MR imaging methods, such as magnetic field strengths (i.e., 1.5T vs 3T), MR vendors, and imagers for measuring the ADC values, which were 4–9, 7, and up to 8 %, respectively [21]. ADCmin had a weak tendency (p=0.09) to differentiate PPT from germinoma. Variability in MR imaging methods might obscure the potentially existing difference between these two tumors, but images that only form a single MR imaging method may not be technically feasible due to the aforementioned reason.

Conclusions

Roles of the quantitative values of CT attenuation, ADC, and SUV were investigated in differentiating between PPTs and germinomas, but none was found useful. However, as was previously reported, age, sex, and calcification patterns had statistically significant differences and were confirmed useful in differentiating these tumors to some degree. In PPTs, we may distinguish pineocytomas and PPTIDs from pineoblastomas because their age distributions are highly different. However, differentiation between pineoblastomas and germinomas is difficult, when there is no calcification.

Conflict of interest We declare that we have no conflict of interest.

References

1. Senft C, Raabe A, Hattingen E, Sommerlad D, Seifert V, Franz K (2008) Pineal parenchymal tumor of intermediate differentiation: diagnostic pitfalls and discussion of treatment options of a rare tumor entity. Neurosurg Rev 31(2):231–236. doi:10.1007/s10143-008-0126-8
2. Smith AB, Rushing EJ, Smirniotopoulos JG (2010) From the archives of the AFIP: lesions of the pineal region: radiologic-pathologic correlation. Radiographics 30(7):2001–2020. doi:10.1148/rg.307105131
3. Han SJ, Clark AJ, Ivan ME, Parsa AT, Perry A (2011) Pathology of pineal parenchymal tumors. Neurosurg Clin N Am 22(3):335–340. doi:10.1016/j.nec.2011.05.006, vii
4. Gaillard F, Jones J (2010) Masses of the pineal region: clinical presentation and radiographic features. Postgrad Med J 86(1020):597–607. doi:10.1136/pgmj.2009.087460
5. Horowitz MB, Hall WA (1991) Central nervous system germinomas. A review. Arch Neurol 48(6):652–657
6. Lekovic GP, Gonzalez LF, Shetter AG, Porter RW, Smith KA, Brachman D, Spetzler RF (2007) Role of Gamma Knife surgery in the management of pineal region tumors. Neurosurg Focus 23(6):E12. doi:10.3171/FOC-07/12/E12
7. Louis D, Ohgaki H, Wiestler O, Cavenee W et al (2007) The 2007 WHO classification of tumours of the central nervous system. 4th edition. World Health Organization. Acta Neuropathol 114(2):97–109
8. Wilson DA, Awad AW, Brachman D, Coons SW, McBride H, Youssef E, Nakaji P, Shetter AG, Smith KA, Spetzler RF, Sanai N (2012) Long-term radiosurgical control of subtotally resected adult pineocytomas. J Neurosurg 117(2):212–217. doi:10.3171/2012.5.JNS1251
9. Pusztaszeri M, Pica A, Janzer R (2006) Pineal parenchymal tumors of intermediate differentiation in adults: case report and literature review. Neuropathology 26(2):153–157
10. Fauchon F, Jouvet A, Paquis P, Saint-Pierre G, Mottolese C, Ben Hassel M, Chauveinc L, Sichez JP, Philippon J, Schlienger M, Bouffet E (2000) Parenchymal pineal tumors: a clinicopathological study of 76 cases. Int J Radiat Oncol Biol Phys 46(4):959–968
11. Tate MC, Rutkowski MJ, Parsa AT (2011) Contemporary management of pineoblastoma. Neurosurg Clin N Am 22(3):409–412. doi:10.1016/j.nec.2011.05.001, ix
12. Ganti SR, Hilal SK, Stein BM, Silver AJ, Mawad M, Sane P (1986) CT of pineal region tumors. AJR Am J Roentgenol 146(3):451–458. doi:10.2214/ajr.146.3.451
13. Smirniotopoulos JG, Rushing EJ, Mena H (1992) Pineal region masses: differential diagnosis. Radiographics 12(3):577–596
14. Korogi Y, Takahashi M, Ushio Y (2001) MRI of pineal region tumors. J Neurooncol 54(3):251–261
15. Reis F, Faria AV, Zanardi VA, Menezes JR, Cendes F, Queiroz LS (2006) Neuroimaging in pineal tumors. J Neuroimaging 16(1):52–58. doi:10.1177/1051228405001514
16. Bakheet SM, Hassounah M, Al-Watban J, Homsi M, Powe J, Larsson S (1999) F-18 FDG PET scan of a metastatic pineoblastoma. Clin Nucl Med 24(3):198–199
17. Park SA, Kim TY, Choi SS, Yang CY, Kim HS, Choi KH (2012) (1)(8)F-FDG PET/CT imaging for mixed germ cell tumor in the pineal region. Clin Nucl Med 37(3):e61–e63. doi:10.1097/RLU.0b013e31823926fc

18. Carrasco JL, Jover L (2003) Estimating the generalized concordance correlation coefficient through variance components. Biometrics 59(4):849–858
19. Busing KA, Kilian AK, Schaible T, Debus A, Weiss C, Neff KW (2008) Reliability and validity of MR image lung volume measurement in fetuses with congenital diaphragmatic hernia and in vitro lung models. Radiology 246(2):553–561. doi:10.1148/radiol.2462062166
20. Dumrongpisutikul N, Intrapiromkul J, Yousem DM (2012) Distinguishing between germinomas and pineal cell tumors on MR imaging. AJNR Am J Neuroradiol 33(3):550–555. doi:10.3174/ajnr.A2806
21. Sasaki M, Yamada K, Watanabe Y, Matsui M, Ida M, Fujiwara S, Shibata E, Acute Stroke Imaging Standardization Group-Japan (ASIST-Japan) Investigators (2008) Variability in absolute apparent diffusion coefficient values across different platforms may be substantial: a multivendor, multi-institutional comparison study. Radiology 249(2):624–630. doi:10.1148/radiol.2492071681

Brain Tumor Pathol
DOI 10.1007/s10014-014-0186-0

ORIGINAL ARTICLE

Development of a robust and sensitive pyrosequencing assay for the detection of *IDH1/2* mutations in gliomas

Hideyuki Arita · Yoshitaka Narita · Yuko Matsushita · Shintaro Fukushima · Akihiko Yoshida · Hirokazu Takami · Yasuji Miyakita · Makoto Ohno · Soichiro Shibui · Koichi Ichimura

Received: 17 February 2014 / Accepted: 30 March 2014

Abstract Assessment of the mutational status of the isocitrate dehydrogenase 1/2 (*IDH1/2*) gene has become an integral part of the standard diagnostic procedure and, therefore, needs to be accurate. This may, however, be compromised by various factors including the method of analysis and a low tumor cell content. We have developed a rapid, sensitive and robust assay to detect all types of mutation in either *IDH1* or *IDH2* using pyrosequencing. The efficacy of detecting mutation was evaluated using a panel of control plasmids representing all the different types of *IDH1/2* mutation and a set of 160 tumor specimens. The sensitivity of the assays was examined by a serial dilution analysis performed on samples containing various ratios of wild-type and mutant alleles. The pyrosequencing assay detected as little as 5 % of mutant alleles for most mutation types, while conventional Sanger sequencing required the presence of at least 20 % of mutant alleles for identifying mutations. The pyrosequencing assay detected *IDH1/2* mutations in three samples which were missed by Sanger sequencing due to their low tumor cell contents. Our assay is particularly useful for the analysis of a large number of specimens as in a retrospective clinical study for example.

Keywords Glioma · *IDH1* · *IDH2* · Pyrosequencing · Mutation detection

Electronic supplementary material The online version of this article (doi:10.1007/s10014-014-0186-0) contains supplementary material, which is available to authorized users.

H. Arita · Y. Narita · Y. Matsushita · Y. Miyakita · M. Ohno · S. Shibui
Department of Neurosurgery and Neuro-Oncology, National Cancer Center Hospital, Tokyo, Japan

H. Arita · S. Fukushima · H. Takami · K. Ichimura (✉)
Division of Brain Tumor Translational Research, National Cancer Center Research Institute, 5-1-1 Tsukiji, Chuo-ku, Tokyo 104-0045, Japan
e-mail: kichimur@ncc.go.jp

A. Yoshida
Department of Pathology and Clinical Laboratories, National Cancer Center Hospital, Tokyo, Japan

H. Takami
Department of Neurosurgery, University of Tokyo, 7-3-1 Hongo, Bunkyo-ku, Tokyo 113-0033, Japan

Introduction

Isocitrate dehydrogenase 1/2 (*IDH1/2*) mutations are regarded as one of the earliest genetic alterations in gliomagenesis, based on the mutation profiles of various subtypes of gliomas as well as primary and recurrent tumors [13, 30]. *IDH1/2* mutations are predominantly found in World Health Organization (WHO) grade II and III gliomas and secondary glioblastomas [3, 12, 30, 31]. Mutations in *IDH1/2* have been associated with longer survival in every histological type or every WHO grade [25, 31]. It is now clear that the *IDH1/2* mutational status defines two biologically and clinically distinct groups of gliomas. Determining the mutational status of *IDH1/2* has become a part of the standard diagnostic procedure and may be used for stratification in clinical trials as it is one of the major prognostic factors in gliomas [28]. It is, therefore, absolutely essential that the status of *IDH1/2* must be accurately and robustly assessed. Various factors may, however, potentially compromise the authenticity of the results; these include the method of analysis, the type of tumor specimen [frozen or formalin-fixed paraffin-embedded (FFPE) samples] and the tumor cell content.

Published online: 19 April 2014